iScience

CellPress
OPEN ACCESS

Article

Radiative cooling for vertical solar panels

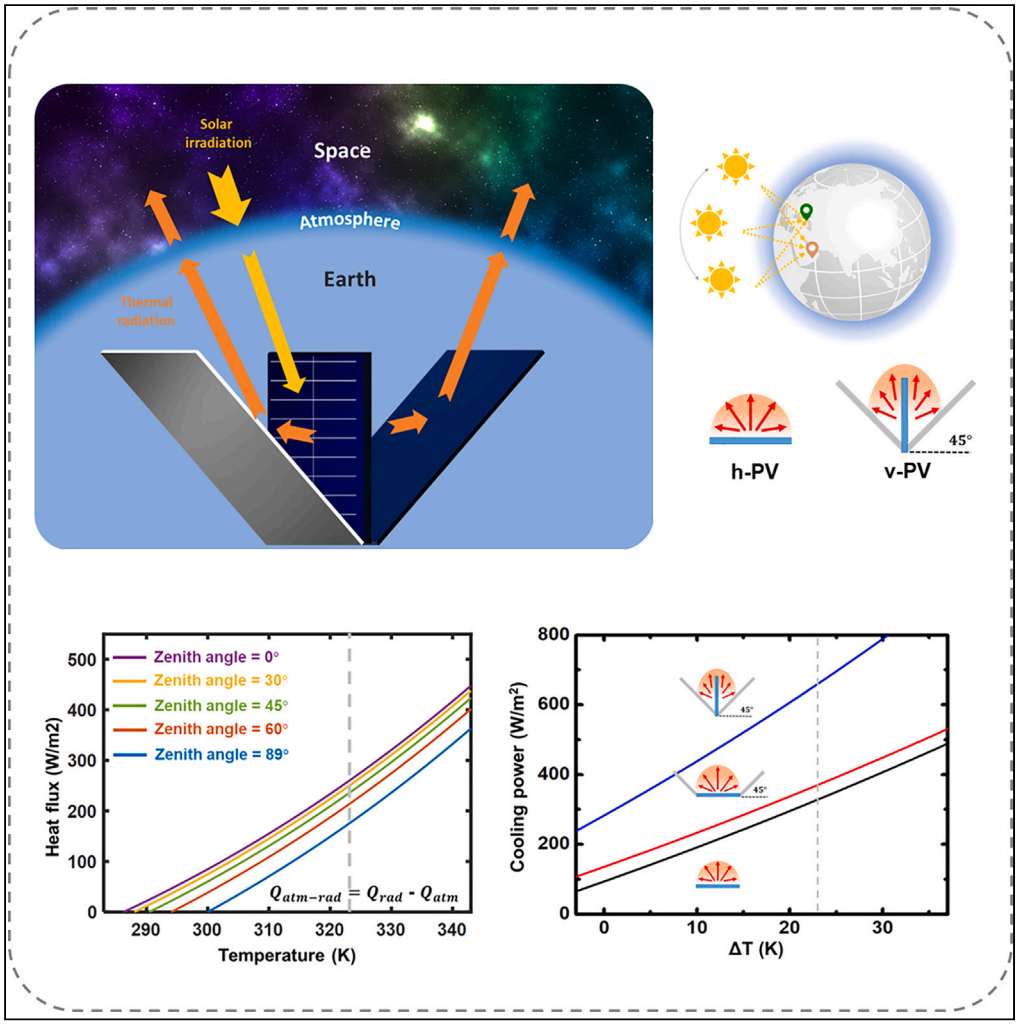

Huangyu Fang, Lyu Zhou, Lujia Xu, Saichao Dang, Stefaan De Wolf, Qiaoqiang Gan

qiaoqiang.gan@kaust.edu.sa

Highlights

A V-shaped radiative cooling architecture for the thermal management of PV modules

A system simultaneously enhances radiative cooling and sunlight collection efficiency

A temperature reduction of 10.6°C obtained under laboratory conditions

16.8% power output enhancement with similar operation temperature in field test

Fang et al., iScience *27*, 108806
February 16, 2024
https://doi.org/10.1016/j.isci.2024.108806

iScience

CellPress
OPEN ACCESS

Article

Radiative cooling for vertical solar panels

Huangyu Fang,[1,2,5] Lyu Zhou,[3,5] Lujia Xu,[1,4] Saichao Dang,[1] Stefaan De Wolf,[1,4] and Qiaoqiang Gan[1,2,4,6,*]

SUMMARY

Radiative cooling presents a method for reducing the operational temperature of solar panels without additional energy consumption. However, its applicability to PV modules has been limited by the thermal properties of existing materials. To overcome these challenges, we introduce a V-shaped design that enhances cooling in vertical PV modules by effectively harnessing thermal radiation from both the front and rear sides, resulting in a substantial temperature reduction of 10.6°C under 1 sun illumination in controlled laboratory conditions. Field tests conducted in warm and humid conditions, specifically in Thuwal, Saudi Arabia, demonstrate a remarkable 15% increase in efficiency while maintaining an operating temperature 0.2°C lower than that of conventional horizontal PV modules, corresponding to a significant 16.8% increase in power output. Our innovative V-shaped design offers a promising thermal strategy suitable for diverse climates, contributing to improved performance and reduced module temperatures, thereby supporting the global pursuit of carbon neutrality.

INTRODUCTION

The development and implementation of renewable energy technologies emerged as a global mission aimed at tackling energy-related challenges such as global warming.[1,2] In 2022, 240 gigawatts (GW) of photovoltaic (PV) system was installed and commissioned during that year, constituting approximately two-thirds of the total global increase in renewable energy capacity.[3] The widespread implementation of renewable energy technologies can be partially attributed to the significant reduction in the cost of PV modules, which has decreased by a factor of ten over the past twenty years.[4] Further development of the global PV market is driven by the levelized cost of energy (LCOE), which is closely related to the cost of material selection, device design, and thermal management.[5] In particular, due to the intense solar irradiance and intrinsic limitations of semiconductor materials, heat generation in PV modules during their operation is inevitable,[6] leading to a reduced power conversion efficiency (PCE), as expressed by the temperature coefficient. Therefore, thermal management in PV modules is one of the most challenging and rewarding tasks.[7] In the case of a crystalline silicon PV module, every 1°C increase in its operating temperature can lead to a decrease in its relative efficiency by approximately 0.25–0.45%, depending on the specific device architecture.[8,9] Moreover, higher operating temperatures can greatly accelerate the failure rate of PV modules due to thermally activated degradation mechanisms, which can further impact the LCOE significantly.[10] Hence, integrating cooling components into PV modules is highly desirable to mitigate these effects. Over the past decade, several promising approaches have been reported, including advanced heat sink architectures,[11] forced convective cooling,[12] water cooling,[13] heat-pipe systems,[14,15] and more recently, hydrogel-based evaporative cooling strategies.[16] However, many of these approaches require additional resources such as electricity and water, leading to increased operational costs. Therefore, exploring cost-effective thermal management techniques has become an essential task, particularly for emerging organic and perovskite solar cells that are more susceptible to thermal degradations.[17,18]

Radiative cooling has been recognized as a promising and eco-friendly cooling mechanism for terrestrial objects. This technique facilitates the dissipation of heat from a terrestrial body to outer space and the ambient environment through thermal radiation, thereby obviating the need for electricity consumption.[19,20] This cooling strategy is particularly suitable for hot PV panels[19–32] as they can fully utilize the atmospheric transparency window within the 8–13 μm range, and even beyond, due to their operating temperatures being significantly higher than the ambient temperature. Prior studies have discussed the development of advanced thermal emitters by utilizing photonic structures,[21,22] porous polymers,[23–25] and metasurfaces[26] that exhibit engineered spectral selectivity for radiative cooling. However, most of these materials process a high scattering tendency in the solar spectrum range, rendering them unsuitable for solar energy harvesting. For effective thermal management of PV panels, a radiative cooler must fulfill two major criteria: (1) high transparency in the wavelength range above the bandgap of the semiconductor material, and (2) strong emissivity in the broadband mid-infrared (MIR) range. Based on these criteria, a silica photonic crystal structure was proposed for use onto a silicon PV absorber, which was able to achieve a temperature reduction of 13°C.[27] Another

[1]Material Science Engineering Program, Physical Science and Engineering Division, King Abdullah University of Science and Technology, Thuwal, Saudi Arabia
[2]Department of Electrical Engineering, The State University of New York at Buffalo, Buffalo, NY 14260, USA
[3]Department of Mechanical Engineering, University of Texas at Dallas, Dallas, TX, USA
[4]KAUST Solar Center (KSC), Physical Sciences and Engineering Division (PSE), King Abdullah University of Science and Technology (KAUST), Thuwal 23955-6900, Saudi Arabia
[5]These authors contributed equally
[6]Lead contact
*Correspondence: qiaoqiang.gan@kaust.edu.sa
https://doi.org/10.1016/j.isci.2024.108806

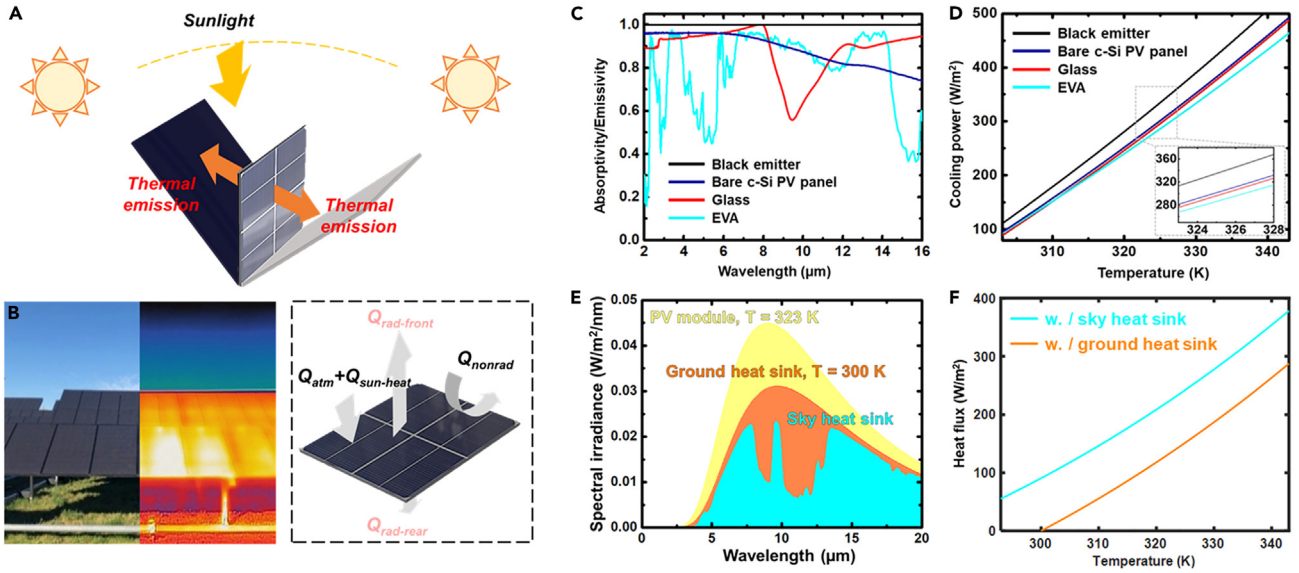

Figure 1. Radiative cooling design for vertical solar panels

(A) Schematic of a PV module with V-shape architecture for efficient radiative cooling.

(B) Left: Photo and infrared image of PV modules operating in the field. Right: schematic of heat transfer in an operating PV module.

(C) Characterized absorptivity/emissivity spectra of PV module components: a bare c-Si PV panel (blue curve), a glass plate (red curve) and an ethylene vinyl acetate (EVA) film (cyan curve).

(D) The estimated radiative cooling power of each component shown in Figure 1C.

(E) The spectral irradiance of a PV module at 323 K (yellow region), ground heat sink at 300K (orange region), and sky heat sink at 300 K (cyan region).

(F) The estimated heat flux of a blackbody with two different heat sinks: the sky heat sink (cyan curve) and the ground heat sink at 300 K (orange curve).

pioneering effort utilized an inverted design featuring a radiative cooler, which successfully reduced the operating temperature of a concentrated PV system by 36°C.[28] In addition, pyramid structures made of silica or polydimethylsiloxane (PDMS) have been reported to significantly improve the cooling efficiency of PV panels by enhancing the broadband thermal emission.[29–31] However, due to the strong MIR absorbance of the encapsulation materials of commercial PV modules (i.e., glass), the actual enhancement of a single-layered radiative cooling coating for commercial modules is not as significant as it is for bare solar cells.[32,33] Furthermore, many planar radiative emitters for sub-ambient cooling show a compromised efficiency in humid areas due to the limited sky transparency in the desired wavelength range, which limits the feasibility of this strategy in outdoor environments.[34] Therefore, a more practical and universally applicable implementation of radiative cooling technologies in PV modules requires a comprehensive exploration that considers cooling materials, optical architectures, and actual environmental conditions simultaneously.

In this study, we introduce a PV module design with V-shaped mirror tailored for proficient thermal management of PV modules (Figure 1A). Our modeling results indicate that by exploiting thermal radiation from both sides of a PV module via the use of a V-shaped design (v-PV), one can achieve multiple benefits of double-sided radiative cooling, beaming effect and convective cooling, hence reducing the PV operating temperature. A comprehensive analytical examination was conducted to investigate the balance between solar irradiance collection efficiency and radiative cooling performance in several different PV configurations. Experiment validations were conducted under different conditions including laboratory environments, high-latitude area, and low-latitude area, and we demonstrated that a modified v-PV system can both reduce the operating temperature and improve the overall PV output. This research presents a pragmatic radiative cooling design that improves the thermal management for future PV modules (e.g., bifacial glass/glass PV modules and new architectures for vertically installed PV modules[35]) by accommodating the actual environmental conditions. It underscores a promising methodology for implementing sustainable thermal management for emerging PV modules that will play a pivotal role in achieving the global carbon neutrality goal.

RESULTS

General design principles

Commercial PV panels are typically installed at specific angles (which are a function of the latitude) or furnished with single axis tracking system to maximize the solar irradiance collection efficiency. However, this approach inevitably results in a heightened solar heating effect, as illustrated by the infrared photograph shown in Figure 1B. For instance, in arid and semi-arid regions, the operating temperature of PV panels can escalate to 50–70C (e.g., [10, 32]). Consequently, the PV panels' lifespan in these areas can be drastically reduced in comparison to those installed in more moderate regions.[36] Implementing cooling mechanisms is crucial for optimizing solar panel operation. In this context,

we first assess the heat flux balance of a PV panel to highlight its potential for radiative cooling. As illustrated in the right panel of Figure 1B, the heat flux in a PV module can be described by:

$$Q_{sun-heat} + Q_{atm} = Q_{rad-front} + Q_{rad-rear} + Q_{nonrad} \quad \text{(Equation 1)}$$

where $Q_{sun-heat}$ represents the converted heat from absorbed sunlight due to sub-bandgap absorption, thermalization losses and recombination and resistance related heat losses; Q_{atm} represents the absorbed thermal radiation from atmosphere; $Q_{rad-front}$ and $Q_{rad-rear}$ is the emitted thermal radiation from the front side and rear side of the PV panel; Q_{nonrad} describes the non-radiative heat flux (mainly introduced by convection of air flow). Most initial studies on PV thermal regulation primarily focused on augmenting non-radiative heat transfer (i.e., Q_{nonrad}) via heat exchangers.[10,37] Meanwhile, the significance of radiative heat transfer ($Q_{rad-front}$ & $Q_{rad-rear}$) received less attention until recently.[38] Despite the usage of various semiconductor materials with different emissivity ε in PV modules (such as crystalline silicon, a variety of organic semiconductors, and perovskites), the choice of encapsulation layers on the front side of PV modules tends to be universal (e.g., glass and a polymeric encapsulant such as ethylene vinyl acetate (EVA)).[39] Therefore, here we first analyzed the radiative cooling power on the front side ($Q_{rad-front}$). We conducted measurements on the absorption spectrum of a bare crystalline silicon (c-Si) PV panel, a glass plate, and an EVA sheet (as seen in –ure 1C). Based on the measured data, we estimated their corresponding radiative cooling power (Figure 1D) using the following equation:

$$Q_{rad-front}(T) = A\int d\Omega \cos(\theta)\int d\lambda I_{BB}(T_{rad},\lambda)\varepsilon_{rad}(\lambda) \quad \text{(Equation 2)}$$

where $\int d\Omega$ is the angular integral of the emitting surface over the hemisphere, $I_{BB}(T,\lambda) = \frac{2hc^2}{\lambda^5}\frac{1}{\exp\left(\frac{hc}{\lambda k_B T}\right)-1}$ is the spectral radiance of a blackbody at a temperature T, where h is Planck's constant, k_B is the Boltzmann constant, c is the speed of light in vacuum, λ is the wavelength, and A is the area of the emitter. ε_{rad} is the spectral emissivity of each component shown in Figure 1C. One can see that both glass and EVA exhibit broadband absorptivity/emissivity over the wavelength range from 2 μm to 16 μm, endowing the panel with efficient radiative heat transfer. When the emitter's temperature is 323 K, their corresponding radiative cooling power $Q_{rad-front}$ is 282 W/m^2 (see the blue curve for a bare c-Si PV panel), 276 W/m^2 (red curve for glass), and 257 W/m^2 (cyan curve for EVA). This cooling power can be enhanced by applying an additional transparent coating with a cooling power up to 314 W/m^2 (i.e., the blackbody limit at 323 K, see the black curve).

In contrast, in the case of most monofacial PV modules, the radiative cooling power on the rear side ($Q_{rad-rear}$) has limited impact due to the relatively small temperature difference between the PV module ($T_{PV} = 323K$) and the ground heat sink ($T_{environ} = 300K$). This is illustrated in the yellow area of Figure 1E. However, in the proposed v-PV design, the thermal radiation emitted from the rear side of the PV module is effectively coupled to the sky, taking advantage of the cold outer space accessible through the atmospheric window. As a result, a significantly larger heat flux is achieved, encompassing both the yellow and orange areas in Figure 1E. To further elucidate the potential for this cooling improvement, we estimated the radiation heat flux from the rear side of the PV module (assuming it to be a blackbody) toward two distinct heat sinks (i.e., the ground and the sky). As depicted in Figure 1F, when the PV module temperature (T_{PV}) is 323K, the net radiation heat flux with a ground heatsink at 300K is estimated to be 137.9 W/m^2, which is notably lower compared to the net radiation heat flux achieved with a sky heatsink (228.6 W/m^2). Notably, as the temperature of PV module continues to increase, such as in low latitude tropical regions, this disparity will further amplify, resulting in a more pronounced net cooling power. In the subsequent section, we will provide laboratory validation to substantiate this enhancement of radiative cooling.

DISCUSSIONS

Laboratory validation of V-shape design

To validate the enhanced radiative cooling in the v-PV system, we conducted experiments following our previously reported indoor radiative cooling settings (Figure 2A, see details in Figure S1). We studied a v-PV configuration (Figure 2B) using a commercial PV module (Heyiarbeit, 18V polycrystalline Mini Solar Panel Module) and investigated its surface temperature and output under five different radiative cooling conditions, as illustrated in Figure 2C: Conditions I and V are the base to show the temperature of the solar panel when the radiative cooling channel is completely blocked by the plate. Conditions II and VI show the single-sided cooling situation when a half of the plate was removed. In this situation, the thermal radiation from one side of the PV panel can be transferred to the cold source. Ultimately, condition III shows the double-sided cooling situation: i.e., thermal radiation from both sides of the PV panel can be transferred to the cold source. To switch between the radiative cooling settings and perform consecutive tests, we alternated between blocking and unblocking thermal radiation from the PV module surfaces every 30 min using an opaque aluminum plate. The first experimental results are shown in Figure 2D, where the PV module was characterized at open-circuit status ($R = \infty$), and the results are summarized in Table 1. As depicted by the blue curve, the PV surface temperature decreased from 53.5 ± 0.1°C (condition I) to 47.9 ± 0.1°C (condition II) and further dropped to 42.7 ± 0.1°C (condition III) with the transition in cooling conditions. Simultaneously, the open-circuit voltage (V_{oc}) measurements showed a corresponding increase from 17.66 V (condition I) to 18.12 V (condition II) and subsequently to 18.50 V (condition III) (see details in Figure S2). Similar results were observed when transitioning from conditions III back to IV and V. Additionally, we conducted a similar examination with the PV module connected to a 1000 Ω resistor to simulate a realistic PV operational scenario. The results are depicted in Figure 2E, and the summarized results can be found in Table 1. Here, the operating temperature of the module decreased from 53.0 ± 0.2°C (condition I) to 47.5 ± 0.1°C

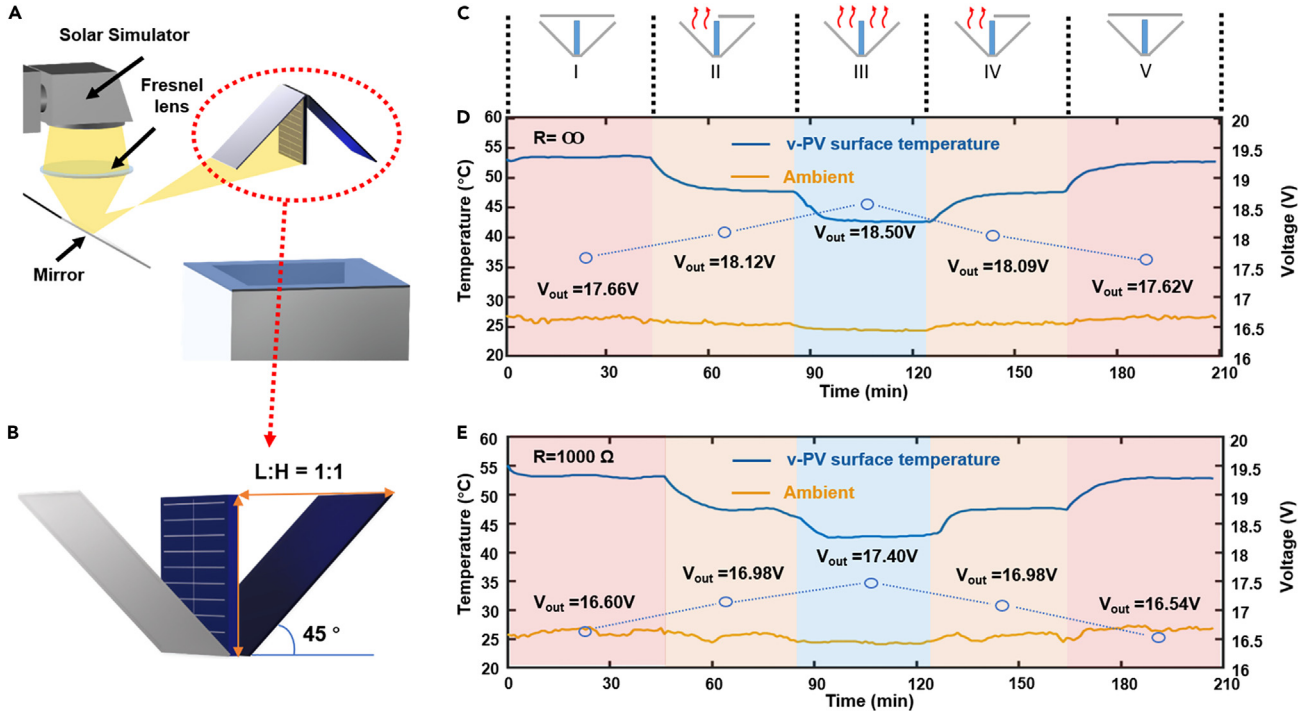

Figure 2. Indoor experimental validation of the radiative cooling channel

(A–C) Schematic of (A) the indoor radiative cooling test setup, (B) the tested v-PV design, and (C) the different cooling conditions throughout the test.

(D and E) The temperature profile and the output of the PV module (D) at open-circuit condition and (E) when connected to a resistor of 1000 Ω as a load. Empty circles represent the output voltage of the PV panel.

(condition II) and subsequently to 42.7 ± 0.1°C (condition III). Correspondingly, the output voltage also changed from 16.60 V (condition I) to 16.98 V (condition II) and then increased further to 17.40 V (condition III). These findings suggest that double-sided radiative cooling can significantly reduce the operating temperature of a PV module by as much as 10.6°C, leading to an increase in the output voltage by 0.80 V. The results validate the efficacy of the v-PV design for proficient thermal management, offering promising implications for improving PV module performance.

Enhanced cooling performance

The laboratory experiments provided compelling evidence for the efficacy of double-sided radiative cooling, showcasing its potential to maintain lower temperatures for PV modules. When implemented in practical outdoor environments, the v-PV design offers additional advantages, such as the beaming effect[40] and enhanced convective cooling, as discussed below. It is important to note that radiative cooling is influenced by weather conditions, in particular humidity.[41] Higher humidity levels can diminish the radiative cooling power due to reduced atmospheric transmittance. To comprehensively assess this impact, we conducted modeling of the atmospheric spectral transmissivity under three distinct humidity conditions, represented by atmospheric water columns (AWC) of 1000 atm-cm, 3000 atm-cm, and 5000 atm-cm, respectively (the standard atmosphere, atm, is a unit of pressure defined as 101325 Pascals). Figure 3A presents the graphical representation of these modeled atmospheric spectral transmissivity conditions. As humidity levels rise, we can observe a clear decrease in atmospheric transmittance. For example, the average atmospheric transmissivity within wavelength range of 8–13 μm at a zenith angle of 0° is 0.79

Table 1. PV performance under different cooling conditions and circuits

	Condition I	Condition II	Condition III	Condition VI	Condition V
$R = \infty$					
Surface temperature	53.5 ± 0.1°C	47.9 ± 0.1°C	42.7 ± 0.1°C	47.4 ± 0.1°C	52.5 ± 0.1°C
Output voltage	17.66V	18.12V	18.50V	18.09V	17.62V
$R = 1000\ \Omega$					
Surface temperature	53.3 ± 0.2°C	47.5 ± 0.1°C	42.7 ± 0.1°C	47.6 ± 0.1°C	52.9 ± 0.1°C
Output voltage	16.60V	16.98V	17.40V	16.98V	16.54V

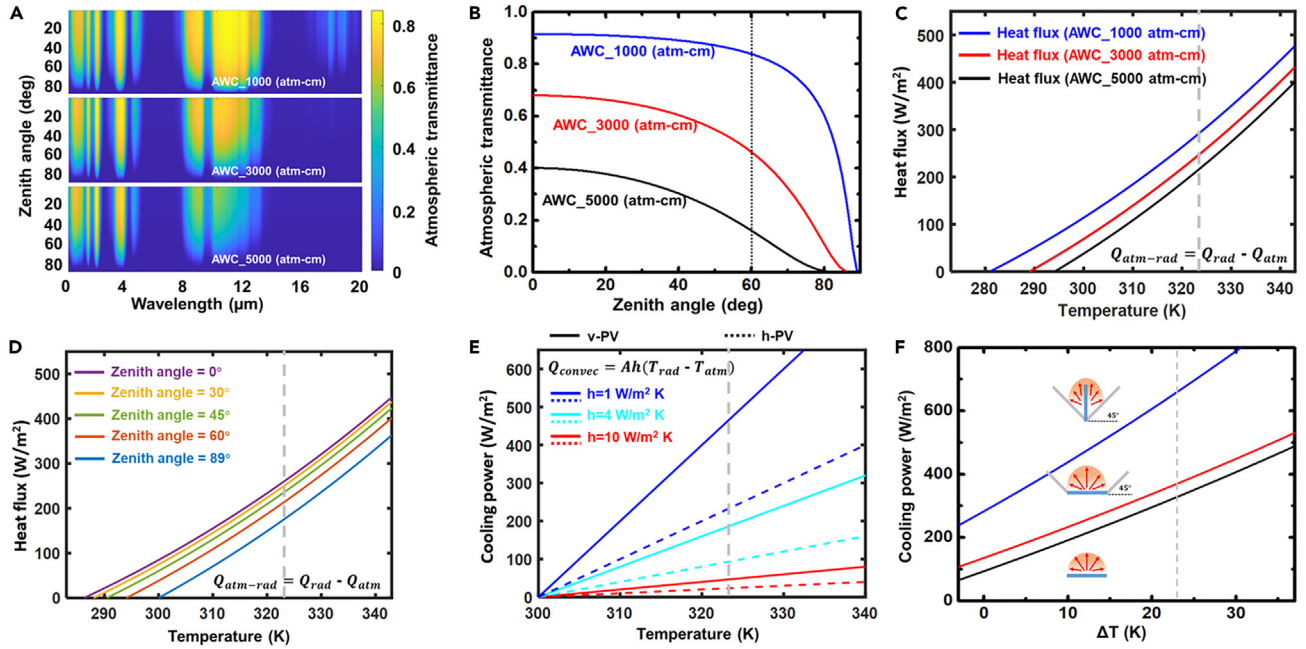

Figure 3. Angle dependence of the radiative cooling effect

(A) Modeled atmospheric spectral transmittance as a function of zenith angle with atmospheric water column of 1000 atm-cm, 3000 atm-cm and 5000 atm-cm, respectively.

(B) Extracted atmospheric transmittance at 10 μm in different humid condition. The blue solid curve represents AWC = 1000 atm-cm, the red solid curve represents AWC = 3000 atm-cm, and the black solid curve corresponds to AWC = 5000 atm-cm.

(C) Estimated heat flux between a PV module and atmosphere under different atmospheric transmittances.

(D) Estimated heat flux between a PV module and atmosphere at different zenith angles.

(E) Estimated convective cooling power of a PV module with two vented surfaces (solid curve) and unvented backside (dash curve) under different non-radiative heat transfer coefficient.

(F) Estimated cooling of a v-PV (blue curve), an h-PV with beaming mirror and unvented backside (red curve) and an h-PV with unvented backside (black curve) as a function of temperature difference between the emitter and ambient. In this modeling, the operational temperature of the PV panels is set at 323K.

with an AWC of 1000 atm-cm, which drops to 0.42 as the AWC reaches 5000 atm-cm. Another significant aspect is that atmospheric transmittance is strongly influenced by the zenith angle. For example, as illustrated by the red curve in Figure 3B, with an AWC of 3000 atm-cm, the atmospheric transmittance at a wavelength of 10 μm is 0.68 at a zenith angle of 0° ($T_{atm}(0°)=0.68$), which drops to 0.47 as the zenith angle increases to 60°($T_{atm}(0°)=0.47$).

To further explore the influence of varying atmospheric transmittance on PV radiative cooling, we conducted an analysis of the heat flux between the atmosphere (at 300 K) and a PV module as a function of the PV surface temperature. Figure 3C illustrates the results for the three different atmospheric transmittance levels corresponding to distinct humidity conditions: for a PV surface temperature of 323 K (represented by the vertical dashed line), the heat flux between the atmosphere and the PV module was found to be 288.2 W/m^2 with an atmospheric water column (AWC) of 1000 atm-cm, 243.2 W/m^2 with an AWC of 3000 atm-cm, and 212.2 W/m^2 with an AWC of 5000 atm-cm. These values clearly demonstrate the impact of varying humidity levels on the heat flux and highlight the importance of considering atmospheric transmittance in the context of PV radiative cooling. We also investigated the heat flux between the atmosphere (AWC_5000 atm-cm) and the PV module by considering the atmospheric transmittance at different zenith angles, as illustrated in Figure 3D. It is evident that the heat flux increases as the zenith angle decreases, which can be attributed to the decrement in atmospheric transmittance at varying zenith angles, as depicted in Figure 3B. When the zenith angle is small (e.g., 0°), the thermal radiation emitted by the PV module can access the colder outer space (at 3 K) through the atmospheric transparency window. However, at high zenith angles (e.g., larger than 80°), it can only exchange heat with the atmosphere (at 300 K). Consequently, the heat flux between the atmosphere and the PV module is 174.2 W/m^2 at a zenith angle of 90°, while it rises to 258.9 W/m^2 at a zenith angle close to 0°. By focusing the beaming of thermal radiation into a narrower range of zenith angles, one can significantly increase the transmitted thermal radiation through the atmosphere and enhance the performance of radiative cooling, particularly in humid environments.

Furthermore, the vertical design of v-PV system also ensures sufficient natural convective cooling by exposing both sides of the PV module to free airflow, which further promotes the thermal management of PV modules when combined with the improved radiative cooling. In contrast to those PV panels mounted on rooftops with unvented backside, the convective cooling power originating from the rear side of the module can reduce its temperature up to 13.2°C.[32] As shown in Figure 3E, we estimated the convective cooling power of PV panel with two exposing surfaces (solid curve) and single exposing surface (dashed curve) using Equation 3

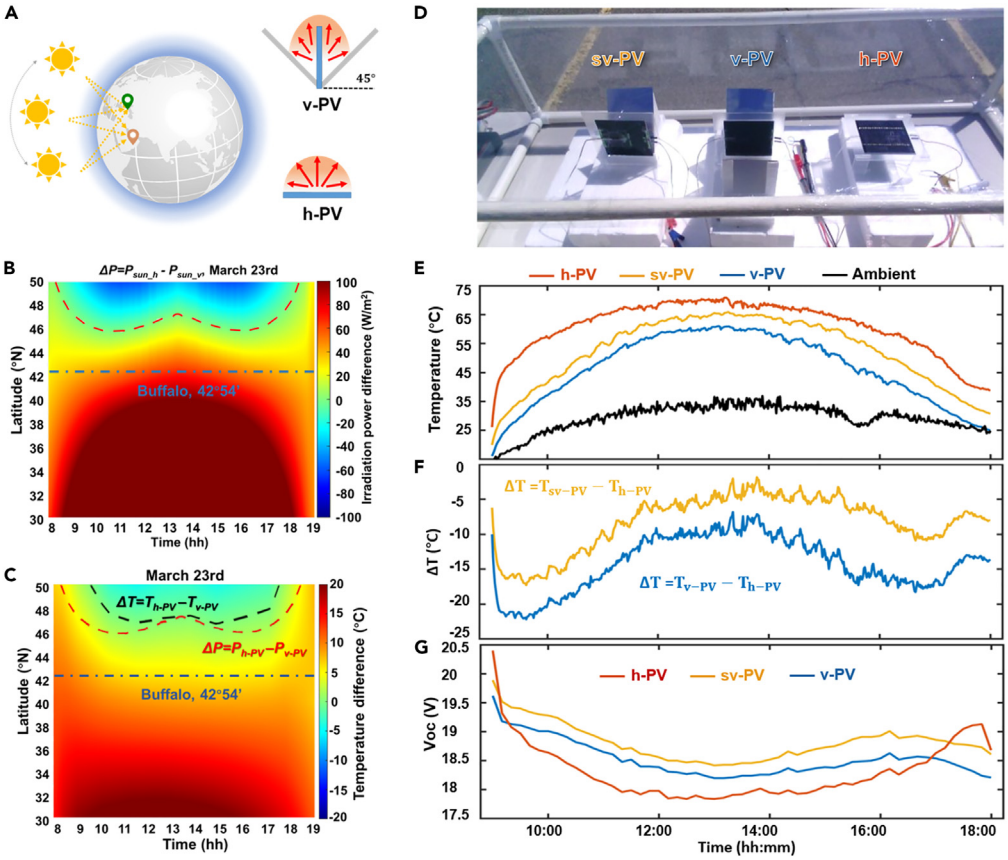

Figure 4. Location dependency of the radiative cooling effect and the outdoor validation

(A) Schematic illustration of the location dependency of the PV module in solar receiving.

(B and C) Modeled received solar irradiation and surface temperature as a function of latitude and time.

(D) Photos of outdoor tests.

(E) The measured temperature of PV modules in h-PV (orange curve), sv-PV (yellow curve) and v-PV (blue curve).

(F) The temperature difference between two v-PV modules and h-PV module.

(G) Measured open-circuit voltage of PV modules in three different setups.

$$Q_{nonrad} = Ah(T_{PV} - T_{amb}) \quad \text{(Equation 3)}$$

For instance, at a non-radiative heat transfer coefficient (h) value of 4 W/m^2, the v-PV system with two vented surfaces demonstrates a superior non-radiative cooling power of 184.0 W/m^2. By incorporating the advantages of double-sided radiative cooling (Figure 2), the beaming effect (Figures 3B–3D), and convective cooling (Figure 3E), the proposed v-PV system offers a significantly enhanced cooling effect compared to h-PV. To illustrate this overall improvement, we modeled the radiative cooling powers of three different scenarios (Figure 3F): a bare h-PV with unvented backside (the bottom inset, represented by the black curve), an h-PV with a beaming mirror and unvented backside (the middle inset, shown by the red curve), and a v-PV (the top inset, depicted by the blue curve). These cooling powers were evaluated as a function of the temperature difference (ΔT) between the PV panel and the environment, assuming a surface temperature of the PV panels at 323 K and varying ambient temperatures. As depicted in Figure 3F, the v-PV design (blue curve) demonstrates a cooling power of 606 W/m^2 when ΔT is 20 K, corresponding to an environmental temperature of 300 K. In contrast, the other two h-PV systems exhibit lower cooling powers, with 295 W/m^2 for h-PV without a beaming mirror (red curve) and 337 W/m^2 for h-PV with a beaming mirror (black curve). The modeling results clearly indicate the significant cooling improvement achieved by the v-PV system. However, when considering practical PV operation, it is essential to evaluate the overall PV output of the v-PV system, as the vertical alignment of PV panels can greatly impact solar irradiance collection efficiency, depending on the installation location. Therefore, in the following section, we will explore the comprehensive benefits of the v-PV design by considering both radiative cooling and solar irradiance collection efficiency.

Overall benefits of the v-PV design

The output of a PV panel is closely tied to its solar irradiance collection efficiency, which is influenced by the panel's orientation and the local environment, as illustrated in Figure 4A. To comprehensively evaluate the advantages of the v-PV design, we conducted modeling studies on

Table 2. PV performance in Buffalo outdoor tests (average value between 12:00 pm and 1:00 pm)

	Surface temperature	V_{oc}	I_{sc}
h-PV	69.6 ± 0.4°C	17.88 ± 0.05 V	52.4 ± 0.8 mA
v-PV	59.5 ± 0.6°C	18.49 ± 0.04 V	31.2 ± 0.6 mA
sv-PV	63.9 ± 0.7°C	18.29 ± 0.06 V	32.8 ± 0.9 mA

the received solar irradiance (P_{sun}) and PV temperature (T_{PV}) for both v-PV and h-PV configurations across different latitudes (30°–50°) and time intervals (8:00 to 19:00 on March 23, 2021, with results for September 23, 2021 shown in Figure S3). The solar trajectory was determined using meteorological data from the ASHRAE weather data center,[42,43] while the radiative cooling effect was modeled concurrently based on a COMSOL library model.[44] The schematic of the two designs under investigation is also depicted in Figure 4A, with the PV panel oriented toward the equator in a north-south direction. The modeling results are presented in Figures 4B and 4C, showcasing the differences in received solar irradiance ($\Delta P=P_{h\text{-}PV} - P_{v\text{-}PV}$) and surface temperature ($\Delta T=T_{h\text{-}PV}-T_{v\text{-}PV}$) between the two designs, respectively. To aid clarity, the boundary where ΔP equals zero is highlighted by the red curves in Figure 4B. Notably, v-PV receives higher solar irradiance than h-PV (i.e., $\Delta P < 0$) at latitudes above 46°, primarily due to its vertical orientation and V-shaped beaming mirror. Moreover, as illustrated by the black dashed curve (the boundary where ΔT equals zero) in Figure 4C, v-PV also maintains lower temperatures than h-PV (i.e., $\Delta T > 0$) within the latitude range of 30°–47.5°, mainly attributable to the reduced solar irradiance absorption. Interestingly, within the latitude range bounded by the red and black dashed curves in Figure 4C (i.e., $\Delta T > 0$ and $\Delta P < 0$), v-PV receives higher solar irradiance while maintaining lower temperatures compared to h-PV, highlighting the stronger radiative cooling power of the v-PV design. These findings indicate that the v-PV design can achieve significantly higher output in high latitude regions such as Europe and Canada.

To validate this enhanced PV output achieved through the proposed v-PV design, we conducted an outdoor test on May 15, 2021, in Buffalo, NY (latitude 42°54′, blue dashed curve shown in Figures 4B and 4C). The v-PV modeled above and a vertically installed PV module without the spectral selective mirror on the rear side (i.e., the single-sided vertical PV, denoted as sv-PV) were tested, as well as an h-PV reference module, as shown in Figure 4D. To minimize the influence of strong convective cooling brought by the local windy environment, we enclosed all three systems within a polyethylene windshield. The ambient temperature was measured inside the windshield away from the PV modules. Throughout the test from 9:00 to 18:00, the relative humidity remained predominantly below 20%, while the solar irradiance averaged around 850 W/m^2 and peaked at 920 W/m^2 at 12:40 (Figure S4). To better visualize the temperature differences among these designs, we plotted the measured PV surface temperature as well as the temperature difference between two v-PV modules and the reference module (h-PV), as shown in Figures 4E and 4F (i.e., $\Delta T=T_{v\text{-}PV}-T_{h\text{-}PV}$ for the blue curve and $\Delta T=T_{sv\text{-}PV}-T_{h\text{-}PV}$ for the orange curve), respectively. One can see that the v-PV (blue curve) exhibited the lowest surface temperature throughout the entire testing period: it reached minimum value at 9:38 ($\Delta T = -22.2$°C). At 12:40, when solar irradiance peaked, v-PV recorded a temperature of 59.6°C, which was still 9°C lower than the h-PV system (68.6°C) and 4.7°C lower than the sv-PV module (64.3°C). These different operating temperatures affected the output of the PV modules, as indicated by the measured open-circuit voltage (V_{oc}). As shown in Figure 4G, v-PV exhibited the highest V_{oc} due to its lower operating temperature.[45] At 12:40, the v-PV achieved a V_{oc} of 18.49 V, surpassing h-PV by 0.59 V (17.9 V) and sv-PV system by 0.20 V (18.29 V). However, it is important to note that the modified v-PV system may experience a significantly smaller short-circuit current (I_{sc}), as indicated in Table 2, primarily due to the reduced received solar irradiance. This limitation becomes more pronounced in the low latitude range, as supported by our modeling results in Figures 4B and 4C. Consequently, for a more effective implementation of the v-PV system, it is essential to carefully design the architecture, taking into account both the double-sided radiative cooling and the optimal PV orientation. In the following section, we will investigate a modified v-PV system specifically tailored for low-latitude areas and elucidate its overall advantages.

Daytime radiative cooling field test in low latitude areas

The power output of a PV module is influenced by both solar irradiance collection efficiency and operating temperature. While the v-PV design demonstrates superior cooling performance in high-latitude regions, its practical implementation is limited by the reduced solar irradiance collection efficiency resulting from the vertical PV alignment. To adapt the v-PV design for low-latitude areas and achieve substantial PV output and cooling performance, we adjusted the v-PV orientation to face the incident sunlight. In this context, the modified h-PV will receive more solar irradiance compared to the unmodified h-PV in Figure 4, which maximizes the solar energy harvesting effect. We modeled three different modified v-PV designs to compare their surface temperature and solar irradiance collection efficiency: a modified h-PV module (bare PV module), a modified sv-PV module (PV module with front mirror only), and a modified v-PV module (PV module with a front mirror and a rear spectrally selective mirror), as depicted in Figure 5A. Using COMSOL Multiphysics, we simulated the surface temperature (TPV) and received solar irradiance (P_{sun}) following the same procedures as in Figure 3. The modeling results are presented in Figures 5B and 5C: At 12:00 p.m., a comparison between the green curve (modified sv-PV) and the orange curve (modified h-PV) in Figure 5B clearly shows that the modified sv-PV collects more solar irradiance due to the solar reflection from the front mirror. Correspondingly, in Figure 5C, the surface temperature of the modified sv-PV is approximately 5.6°C higher than that of the modified h-PV. On the other hand, when comparing the modified sv-PV to the modified v-PV, both systems receive the same amount of solar irradiation (indicated by the overlapping orange and blue curves in Figure 5B). However, the modified v-PV exhibits a surface temperature that is 3.2°C lower than the modified sv-PV due to the higher radiative cooling power from the rear side of the modified v-PV. Therefore, with this modified v-PV design, it is possible to achieve

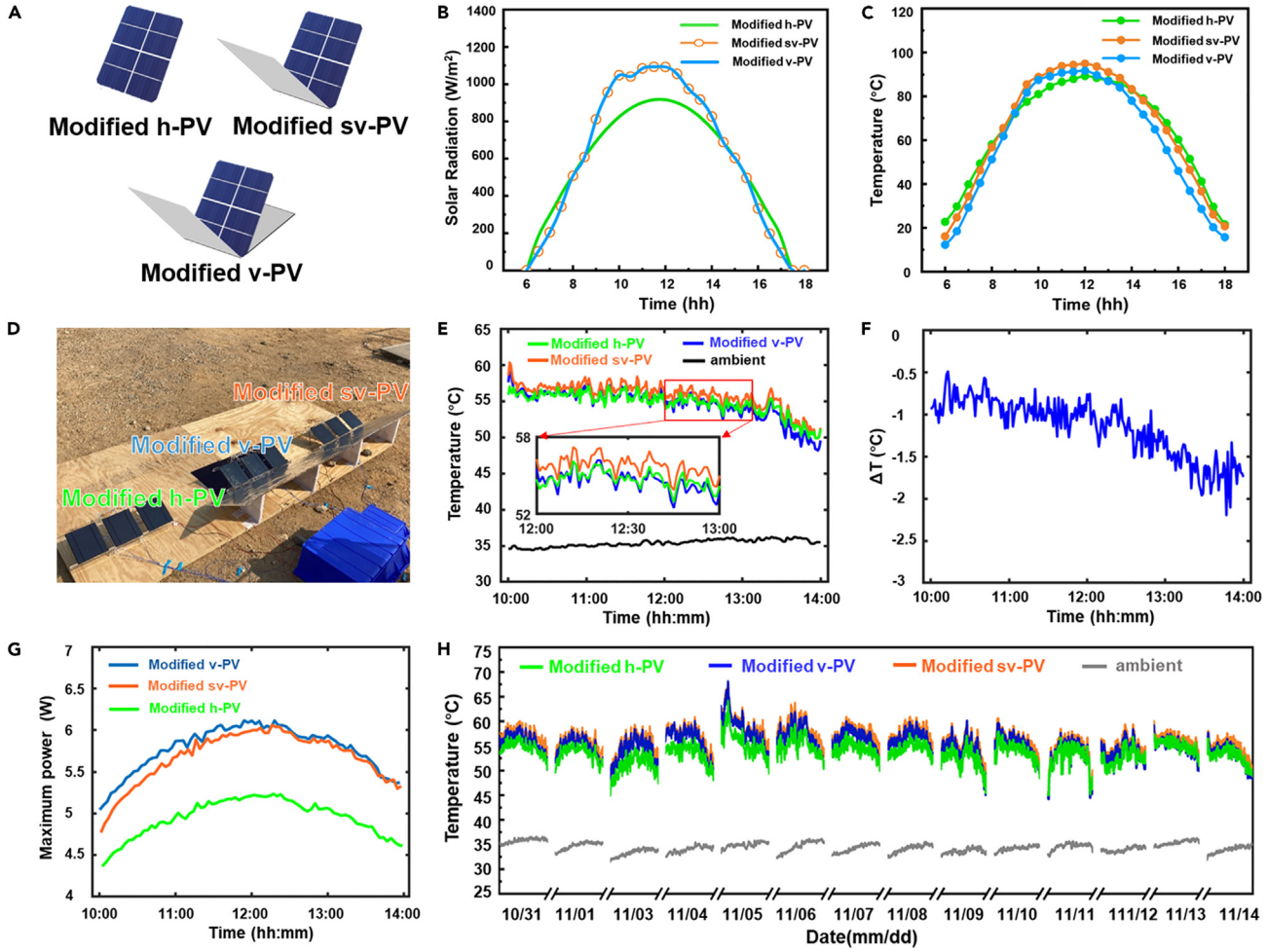

Figure 5. Long term outdoor tests

(A) Illustration that shows the three modified PV systems studied in this section.

(B and C) Simulated result of received solar irradiation (B) and temperature (C) on the front surface of each PV modules.

(D) The photo of the outdoor test in Thuwal, Saudi Arabia.

(E) The measured rear-side PV temperatures of three PV systems (green curve: modified h-PV, orange curve: modified sv-PV, blue curve: modified v-PV, gray curve: ambient) and (F) the temperature difference between modified sv-PV and modified v-PV.

(G) The maximum power of three PV systems.

(H) Temperature profiles of the three PV systems in a continuous outdoor cooling test.

a lower operating temperature while maintaining the maximum solar irradiance collection efficiency in low-latitude areas, making it more practical for real-world PV applications.

To validate the practical benefits of the modified v-PV design in terms of PV output, we conducted outdoor experiments in Thuwal, Saudi Arabia (latitude 22°18′N) on Nov. 13, 2022. Similar to Figure 4, two modified v-PV systems described in Figure 5A were tested and their performance were compared to a modified h-PV reference as depicted in Figure 5D. To minimize experimental errors arising from the modules and environmental factors, we used a larger commercial solar panel (ALLPOWERS, 5V Solar Cell) and each set included three identical systems. The temperature profiles of each system were measured and presented in the upper panel of Figure 5E, and the results are summarized in Table 3. Additionally, the temperature difference between the modified sv-PV and modified v-PV is illustrated in Figure 5F. The measured temperature results align closely with the modeling results presented in Figure 5B, indicating the following: (1) the modified h-PV consistently exhibited the lowest temperature among the three groups due to the lowest received solar irradiance, (2) the modified sv-PV consistently maintained a temperature slightly higher than the modified v-PV by approximately 0.5°C–2°C, primarily attributed to the enhanced cooling power conferred by the v-PV design. As summarized in Table 3, between 10:00 to 14:00, the average solar irradiance on modified v-PV is 1065 W/m^2, which is 136 W/m^2 (15% of the solar irradiance on modified h-PV) higher than the modified h-PV due to the aluminum mirror on the front side. In the meantime, the average surface temperature was 54.5°C for the modified v-PV, slightly lower than the 54.7°C for the modified h-PV and 55.7°C for the modified sv-PV. Correspondingly, the measured open-circuit voltage was 5.59 V for the modified

Table 3. PV performance in Thuwal outdoor tests between 10:00 to 14:00 on November 13, 2022

	Surface temperature (°C)	V_{oc} (V)	I_{sc} (A)	Solar irradiance (W/m^2)	P_{max} (W)	Conversion efficiency (%)	Degradation rate (%/year)	LCOE (USD/kWh)
Modified h-PV	54.7 ± 0.65	5.55 ± 0.02	1.47 ± 0.08	929	4.94 ± 0.22	10.31	0.943	0.3919
Modified v-PV	54.5 ± 0.78	5.59 ± 0.02	1.60 ± 0.11	1065	5.77 ± 0.27	10.53	0.900	0.3419
Modified sv-PV	55.7 ± 0.74	5.56 ± 0.02	1.65 ± 0.10	1055	5.67 ± 0.30	10.41	1.042	0.3667

v-PV, slightly higher than the 5.55 V for the modified h-PV and 5.56 V for the modified sv-PV. These findings align with the surface temperatures depicted in both the modeling results of Figure 5C and the measured outcomes of Figure 5E. They collectively affirm the efficacy of the modified v-PV design in achieving improved cooling performance while sustaining PV output when compared to the modified h-PV. In essence, this design enhances solar irradiance collection efficiency by 15% without compromising the maintenance of a similar operating temperature.

Furthermore, the modified v-PV also exhibited a short-circuit current of 5.77 A, which was close to the 5.67 A of the modified sv-PV and significantly higher than the 4.94 A of the modified h-PV. These observations align well with the modeling results of received solar irradiance shown in Figure 5B and the measured solar irradiance on the PV module indicated in Table 3. These findings suggest that the modified v-PV design can both reduce the surface temperature and maintain appreciable output power. As illustrated in Figure 5G, between 12:00 to 14:00, the average measured maximum power output of the modified sv-PV was 5.67 W, which is 14.7% higher than the modified h-PV (4.94 W) (i.e., (5.67–4.94)/4.94 × 100%). Meanwhile, the modified v-PV was 5.77 W, which is 16.8% higher [i.e., (5.77–4.94)/4.94 × 100%). Consequently, the proposed v-PV design not only leads to improved conversion efficiency (from 10.31% to 10.53%) but also a decreased degradation rate (reduction of 0.043%/year), as summarized in Table 3. Considering the economic analysis presented in Table 3, the modified v-PV is projected to exhibit a lower LCOE of 0.3411 USD/kWh, representing a 13.0% decrease compared to the modified h-PV. These results highlight the practical advantages of the modified v-PV design, making it a promising solution for achieving both enhanced cooling performance and improved PV output in real-world applications.

To demonstrate the stability of the modified v-PV design, we conducted a 15-day continuous test in Thuwal from October 31 to November 14, 2022, as shown in Figure 5H and Table S1. While it is apparent that the modified v-PV consistently maintained a slightly higher temperature throughout the test period when compared to the modified h-PV (depicted by the blue and green curves, respectively), it is noteworthy that the modified v-PV consistently outperformed with a noteworthy average power output difference of 0.7 W. This superior performance is attributed to the heightened solar irradiance collection efficiency and the more robust cooling capabilities of the modified v-PV in contrast to the modified h-PV. Notably, even when compared to a modified sv-PV, which received a similar solar irradiance, the modified v-PV exhibited a higher output and only a slightly lower temperature. Implementing this modified v-PV design in tropical regions like Saudi Arabia can reliably reduce the operating temperature of PV modules, thereby enhancing the conversion efficiency and extending the module's lifetime. This advancement contributes to the global energy transition from fossil-based sectors to renewable energy sources.[46]

Conclusion

Our study introduces a pioneering V-shaped architecture for the enhanced thermal management of PV modules. By integrating a V-shaped reflective structure with the PV module, we successfully augment PV cooling by capitalizing on the benefits of double-sided radiative cooling, the beaming effect, and intensified convective cooling. Our indoor cooling tests showcased a substantial reduction of 10.6°C in operating temperature within controlled laboratory conditions. Additionally, the calculated cooling power across various atmospheric scenarios corroborated its effectiveness. Through a comprehensive analysis that integrates solar irradiance collection efficiency and radiative cooling performance, we underscored the holistic advantages of the v-PV approach for PV operations, bridging simulation and experimental outcomes. Meticulously aligned, the v-PV system exhibited superior performance in both power output and operating temperature. Remarkably, when solar irradiance collection efficiency of the solar panel was enhanced by 15% compared to an aligned, horizontal PV module, the proposed v-PV system maintained a slightly lowered operating temperature of 0.2°C, corresponding to an increase in the maximum power output by 16.8%. This dual-sided cooling strategy seamlessly lends itself to integration with bifacial PV modules, which are more susceptible to heat-induced degradation (e.g.,[47,48]). Moreover, coupling the V-shaped design with an additional radiative cooling coating holds the potential to further optimize radiative cooling effects on emerging vertical bifacial PV modules (e.g.,[35,49,50]). Additionally, there is a growing need for a more comprehensive array design that takes into account the impact of row spacing and height. This renders it a highly promising approach for future PV thermal management endeavors and will yield invaluable insights into amplifying PV module efficiency and durability, contributing significantly to the advancement of sustainable solar energy solutions.

Limitations of the study

The efficiency of radiative cooling is dependent on environmental factors like humidity and cloud cover. In humid or cloudy conditions, the effectiveness of radiative cooling might decrease because of the impediment of heat transfer between emitter and outer space. Additionally,

the impact of radiation angles on the cooling effect is notable, implying that these cooling systems will vary across different latitudes. Furthermore, add-ons or materials introduced for radiative cooling may require periodic maintenance, such as removal of surface deposits of sand and dust, to ensure their long-term durability in a variety of weather conditions.

STAR★METHODS

Detailed methods are provided in the online version of this paper and include the following:

- KEY RESOURCES TABLE
- RESOURCE AVAILABILITY
  - Lead contact
  - Materials availability
  - Data and code availability
- METHOD DETAILS
  - Estimation of heat flux between a blackbody and a heat sink at different temperatures
  - Experiments design: indoor test
  - Sunlight illumination
  - Radiative cooling
  - V-PV system
  - Estimation of atmospheric spectral transmissivity under three distinct humidity
  - COMSOL modeling of corresponding modified PV system designs
  - Experiments design: Outdoor test
  - Estimation of the benefits of radiative cooling on PV modules

SUPPLEMENTAL INFORMATION

Supplemental information can be found online at https://doi.org/10.1016/j.isci.2024.108806.

ACKNOWLEDGMENTS

This work was partially supported by a baseline from the King Abdullah University of Science and Technology (BAS/1/1415-01) and the Carbon Circulate Initiative (REI/1/5218-01).

AUTHOR CONTRIBUTIONS

Q.G. conceived the idea and supervised this project. F.H. and L.Z. conducted the experiment. All authors contributed to the analysis of the experimental results and modeling. F.H., L.Z., and Q.G. wrote the manuscript. All authors reviewed and revised the manuscript.

DECLARATION OF INTERESTS

The authors declare no competing interests.

Received: August 17, 2023
Revised: November 8, 2023
Accepted: January 2, 2024
Published: January 4, 2024

REFERENCES

1. Rogelj, J., Huppmann, D., Krey, V., Riahi, K., Clarke, L., Gidden, M., Nicholls, Z., and Meinshausen, M. (2019). A new scenario logic for the Paris Agreement long-term temperature goal. Nature *573*, 357–363.
2. Haegel, N.M., Verlinden, P., Victoria, M., Altermatt, P., Atwater, H., Barnes, T., Breyer, C., Case, C., De Wolf, S., Deline, C., et al. (2023). Photovoltaics at multi-terawatt scale: Waiting is not an option. Science *380*, 39–42.
3. IEA (2023). Snapshot 2023 (IEA).
4. ITRPV (2018). International Technology Roadmap for Photovoltaic, 9th edition.
5. Branker, K., Pathak, M., and Pearce, J. (2011). A review of solar photovoltaic levelized cost of electricity. Renew. Sustain. Energy Rev. *15*, 4470–4482.
6. Xu, L., Aydin, E., De Bastiani, M., Babics, M., Liu, J., Azmi, R., Alamer, M., Salvador, M.F., Liu, W., Allen, T., et al. (2023). Parasitic heating of perovskite- and silicon-based photovoltaics. Adv. Energy Mater. *13*.
7. Du, D., Darkwa, J., and Kokogiannakis, G. (2013). Thermal management systems for Photovoltaics (PV) installations: A critical review. Sol. Energy *97*, 238–254.
8. Zhu, L., Raman, A.P., and Fan, S. (2015). Radiative cooling of solar absorbers using a visibly transparent photonic crystal thermal blackbody. Proc. Natl. Acad. Sci. USA *112*, 12282–12287.
9. Skoplaki, E., and Palyvos, J.A. (2009). On the temperature dependence of photovoltaic module electrical performance: A review of efficiency/power correlations. Sol. Energy *83*, 614–624.
10. Xu, L., Liu, W., Liu, H., Ke, C., Wang, M., Zhang, C., Aydin, E., Al-Aswad, M., Kotsovos, K., Gereige, I., et al. (2021). Heat generation and mitigation in silicon solar cells and modules. Joule *5*, 631–645.
11. Luque, A., and Araújo, A. (1989). Solar Cells and Optics for Photovoltaic Concentration (Adam Hilger Series on Optics and Optoelectronics. (Institute of Physics Publishing).

12. Teo, H., Lee, P., and Hawlader, M. (2012). An active cooling system for photovoltaic modules. Appl. Energy *90*, 309–315.
13. Mittelman, G., Kribus, A., and Dayan, A. (2007). Solar cooling with concentrating photovoltaic/thermal (CPVT) systems. Energy Convers. Manag. *48*, 2481–2490.
14. Akbarzadeh, A., and Wadowski, T. (1996). Heat pipe-based cooling systems for photovoltaic cells under concentrated solar radiation. Appl. Therm. Eng. *16*, 81–87.
15. ROYNE, A., DEY, C., and MILLS, D. (2005). Cooling of photovoltaic cells under concentrated illumination: a critical review. Sol. Energy Mater. Sol. Cell. *86*, 451–483.
16. Li, R., Shi, Y., Wu, M., Hong, S., and Wang, P. (2020). Photovoltaic panel cooling by atmospheric water sorption–evaporation cycle. Nat. Sustain. *3*, 636–643.
17. Bristow, N., and Kettle, J. (2018). Outdoor organic photovoltaic module characteristics: Benchmarking against other PV technologies for performance, calculation of Ross coefficient and outdoor stability monitoring. Sol. Energy Mater. Sol. Cell. *175*, 52–59.
18. Liu, L., Huang, S., Lu, Y., Liu, P., Zhao, Y., Shi, C., Zhang, S., Wu, J., Zhong, H., Sui, M., et al. (2018). Grain-Boundary "Patches" by In Situ Conversion to Enhance Perovskite Solar Cells Stability. Adv. Mater. *30*, 1800544.
19. Granqvist, C.G., and Hjortsberg, A. (1980). Surfaces for radiative cooling: Silicon monoxide films on aluminum. Appl. Phys. Lett. *36*, 139–141.
20. Fan, S., and Li, W. (2022). Photonics and thermodynamics concepts in radiative cooling. Nat. Photon. *16*, 182–190.
21. Raman, A.P., Anoma, M.A., Zhu, L., Rephaeli, E., and Fan, S. (2014). Passive radiative cooling below ambient air temperature under direct sunlight. Nature *515*, 540–544.
22. Zhao, B., Lu, K., Hu, M., Liu, J., Wu, L., Xu, C., Xuan, Q., and Pei, G. (2022). Radiative cooling of solar cells with micro-grating photonic cooler. Renew. Energy *191*, 662–668.
23. Hsu, P.C., Song, A.Y., Catrysse, P.B., Liu, C., Peng, Y., Xie, J., Fan, S., and Cui, Y. (2016). Radiative human body cooling by nanoporous polyethylene textile. Science *353*, 1019–1023.
24. Mandal, J., Fu, Y., Overvig, A.C., Jia, M., Sun, K., Shi, N.N., Zhou, H., Xiao, X., Yu, N., and Yang, Y. (2018). Hierarchically porous polymer coatings for highly efficient passive daytime radiative cooling. Science *362*, 315–319.
25. Yin, X., Yang, R., Tan, G., and Fan, S. (2020). Terrestrial radiative cooling: Using the cold universe as a renewable and sustainable energy source. Science *370*, 786–791.
26. Zou, C., Ren, G., Hossain, M.M., Nirantar, S., Withayachumnankul, W., Ahmed, T., Bhaskaran, M., Sriram, S., Gu, M., and Fumeaux, C. (2017). Metal-Loaded Dielectric Resonator Metasurfaces for Radiative Cooling. Adv. Opt. Mater. *5*, 1700460.
27. Zhu, L., Raman, A.P., and Fan, S. (2015). Radiative cooling of solar absorbers using a visibly transparent photonic crystal thermal blackbody. Pest. Artic. News Summ. *112*, 12282–12287.
28. Wang, Z., Kortge, D., Zhu, J., Zhou, Z., Torsina, H., Lee, C., and Bermel, P. (2020). Lightweight, Passive Radiative Cooling to Enhance Concentrating Photovoltaics. Joule *4*, 2702–2717.
29. Lee, E., and Luo, T. (2019). Black body-like radiative cooling for flexible thin-film solar cells. Sol. Energy Mater. Sol. Cell. *194*, 222–228.
30. Wang, K., Luo, G., Guo, X., Li, S., Liu, Z., and Yang, C. (2021). Radiative cooling of commercial silicon solar cells using a pyramid-textured PDMS film. Sol. Energy *225*, 245–251.
31. Zhu, L., Raman, A., Wang, K.X., Anoma, M.A., and Fan, S. (2014). Radiative cooling of solar cells. Optica *1*, 32–38.
32. Li, Z., Ahmed, S., and Ma, T. (2021). Investigating the Effect of Radiative Cooling on the Operating Temperature of Photovoltaic Modules. Sol. RRL *5*, 2000735.
33. Kumar, A., and Chowdhury, A. (2019). Reassessment of different antireflection coatings for crystalline silicon solar cell in view of their passive radiative cooling properties. Sol. Energy *183*, 410–418.
34. Dong, M., Chen, N., Zhao, X., Fan, S., and Chen, Z. (2019). Nighttime radiative cooling in hot and humid climates. Opt Express *27*, 31587–31598.
35. Reker, S., Schneider, J., and Gerhards, C. (2022). Integration of vertical solar power plants into a future German energy system. Smart Energy *7*, 100083.
36. Wang, W., Aleid, S., Shi, Y., Zhang, C., Li, R., Wu, M., Zhuo, S., and Wang, P. (2021). Integrated solar-driven PV cooling and seawater desalination with zero liquid discharge. Joule *5*, 1873–1887.
37. Shen, L., Li, Z., and Ma, T. (2020). Analysis of the power loss and quantification of the energy distribution in PV module. Appl. Energy *260*, 114333.
38. Sato, D., and Yamada, N. (2019). Review of photovoltaic module cooling methods and performance evaluation of the radiative cooling method. Renew. Sustain. Energy Rev. *104*, 151–166.
39. Michael, J.J., Gary, M.T., Kent, J.M., Tom, E.K.C., and Theodore, T.B. (2007). Acetic acid production and glass transition concerns with ethylene-vinyl acetate used in photovoltaic devices. Elsevier *91*, 315–329.
40. Zhou, L., Song, H., Liang, J., Singer, M., Zhou, M., Stegenburgs, E., Zhang, N., Ng, T.K., Yu, Z., Ooi, B., and Gan, Q. (2019). All-day radiative cooling using beam-controlled architectures. In Conference on Lasers and Electro-Optics, OSA Technical Digest (Optica Publishing Group). paper ATh1I.2.
41. Harrison, A.W. (1981). Effect of atmospheric humidity on radiation cooling. Sol. Energy *26*, 243–247.
42. COMSOL Documentation. External Radiation Source. (accessed May 25, 2021)
43. ASHRAE. ASHRAE Climatic Design Conditions 2009/2013/2017/2021.
44. COMSOL. Radiative Cooling. Application Gallery. (accessed May 25, 2021)
45. N. H. Zaini, M. Z. Ab Kadir, M. Izadi, N. I. Ahmad, M. A. M. Radzi and N. Azis, "The Effect Of Temperature On A Mono-Crystalline Solar Pv Panel," 2015 IEEE Conference on Energy Conversion (CENCON), Johor Bahru, Malaysia, 2015, pp. 249-253. doi:
46. Renewable Energy in the Context of Sustainable Development (2012). Renewable energy sources and climate change mitigation: Special report of the intergovernmental panel on climate change (Cambridge University Press).
47. Cote, B.M., Slauch, I.M., Deceglie, M.G., Silverman, T.J., and Ferry, V.E. (2021). Light Management in Bifacial Photovoltaics with Spectrally Selective Mirrors. ACS Appl. Energy Mater. *4*, 5397–5402.
48. Lamers, M.W.P.E., Özkalay, E., Gali, R.S.R., Janssen, G.J.M., Weeber, A.W., Romijn, I.G., and Van Aken, B.B. (2018). Temperature effects of bifacial modules: Hotter or cooler? Sol. Energy Mater. Sol. Cell. *185*, 192–197.
49. Kopecek, R., and Libal, J. (2018). Towards large-scale deployment of bifacial photovoltaics. Nat. Energy *3*, 443–446.
50. Zheng, L., Xuan, Y., Wang, J., Bao, S., Liu, X., and Zhang, K. (2022). Inverted perovskite/silicon V-shaped tandem solar cells with 27.6% efficiency via self-assembled monolayer-modified nickel oxide layer. J. Mater. Chem. A *10*, 7251–7262.
51. Dewpt_vpd_calculations. oregonstate.edu.
52. MODTRAN Demo. Spectral Sciences Inc.
53. Granqvist, C.G., and Hjortsberg, A. (1981). Radiative cooling to low temperatures: General considerations and application to selectively emitting SiO films. J. Appl. Phys. *52*, 4205–4220.
54. Radiative Cooling, Application Gallery, COMSOL.
55. Sun's Radiation Effect on Two Coolers Placed under a Parasol, Application Gallery, COMSOL.
56. Elevation Angle, PVeducation.
57. Kimball, G.M., Yang, S., and Saproo, A. (2016). Global Acceleration Factors For Damp Heat Tests Of PV Modules. In IEEE 43rd Photovoltaic Specialists Conference (PVSC), 0101-0105.
58. Comparative PV LCOE Calculator, Photovoltaic Research, NREL.
59. 0.3mm Aluminum Mirror High Reflective for Lighting PVD Coated, Fujian Summit Metallic Materials Science & Technology Co., Ltd.
60. TINOX Blue Selective Coating for Solar Collector, Fujian Summit Metallic Materials Science & Technology Co., Ltd.
61. ALLPOWERS 50 Pieces 2.5W 5V/500mAh Solar Panel DIY Battery Charger Kit Mini Encapsulated Solar Cell Epoxy for Battery Power LED 130x150mm (Solar Panel Only), ALLPOWERS, Amazon.

STAR★METHODS

KEY RESOURCES TABLE

REAGENT or RESOURCE	SOURCE	IDENTIFIER
Software and algorithms		
MATLAB	MathWorks	https://www.mathworks.com
Radiative Cooling Modeling	COMSOL Multiphysics	https://www.comsol.com/model/radiative-cooling-75021
Sun's Radiation Effect on Two Coolers Placed Under a Parasol Modeling	COMSOL Multiphysics	https://www.comsol.com/model/sun-s-radiation-effect-on-two-coolers-placed-under-a-parasol-12825
Other		
13cm*15cm 5V 2.5W solar panel	ALLPOWERS	https://www.amazon.com/dp/B0BJVLT9NN/ref=twister_B0BMK8K14G?_encoding=UTF8&th=1
10cm*10cm 18V 1.2W solar panel	Heyiarbeit	https://www.amazon.com/gp/product/B09879S71G/ref=ox_sc_act_title_2?smid=A28DZI5I4PJFY4&psc=1
Aluminum mirror	Fujian Summit Metallic Materials Science & Technology Co., Ltd.	https://www.alibaba.com/product-detail/0-3mm-aluminum-mirror-high-reflective_1600493452196.html?spm=a2700.shop_plgr.41413.10.5a2974adNxiw8R
Selective reflective mirror	Fujian Summit Metallic Materials Science & Technology Co., Ltd.	https://www.alibaba.com/product-detail/0-3mm-High-Selective-Solar-Absorber_62166869600.html?spm=a2700.shop_plgr.41413.28.5a2974adNxiw8R

RESOURCE AVAILABILITY

Lead contact

Further information and requests for resources and reagents should be directed to and will be fulfilled by the lead contact, Qiaoqiang Gan (qiaoqiang.gan@kaust.edu.sa).

Materials availability

This study did not generate new materials.

Data and code availability

(1) All data reported in this paper will be shared by the lead contact upon request.
(2) No original code was used.
(3) Any additional information required to reanalyze the data reported in this paper is available from the lead contact upon request.

METHOD DETAILS

Estimation of heat flux between a blackbody and a heat sink at different temperatures

The heat flux between a blackbody (T_{PV} at 323 K) and a heat sink ($T_{heat-sink}$) can be estimated using Stefan-Boltzmann law:

$$Q_{rad-rear} = \epsilon\sigma\left(T_{pv}^4 - T_{heat-sink}^4\right) \quad \text{(Equation 4)}$$

Here ϵ is the emissivity of the blackbody (equals to 1), σ is the Stefan-Boltzmann constant. When the backside of a PV module faces the ground, the temperature of heat sink, i.e., ground, is considered at 300 K. Therefore, the obtained Q_{rad} under this circumstance is 137.9 W/m^2. When the backside of a PV module faces the sky, the heat flux is transferring between the PV module and the sky. However, the effective sky temperature T_{sky} normally is different from the ambient temperature T_{amb}. Therefore, here we followed the previous study and estimated T_{sky} using the equation below

$$T_{sky} = \epsilon_{sky}^{1/4} T_{amb}. \quad \text{(Equation 5)}$$

Here ϵ_{sky} is the effective atmospheric emissivity. Under clear sky conditions, ϵ_{sky} can be estimated using the model developed by Berhahl and Martin,[51] as shown below

$$\epsilon_{sky} = 0.711 + 0.56\left(\frac{T_d}{100}\right) + 0.711\left(\frac{T_d}{100}\right)^2. \quad \text{(Equation 6)}$$

Here T_d is the ambient dewpoint temperature, which is estimated using the Magnus-Tetens Approximation shown below[1]

$$T_d = \frac{237.7r}{17.27 - r}, \quad \text{(Equation 7)}$$

$$r = \frac{17.27(T_{amb} - 273)}{237.7 + T_{amb} - 273} + \ln(RH). \quad \text{(Equation 8)}$$

In this estimation, we assumed the relative humidity RH at 30% and ambient temperature T_{amb} at 300K. Following the procedure above, the calculated heat flux between the blackbody and the atmosphere $Q_{rad-back}$ is 228.6 W/m^2.

Experiments design: indoor test

We followed our previous work and designed an indoor radiative cooling test. The setup is mainly composed of two parts: a sunlight directing optic path and a radiative cooling channel, as shown in Figure S1.

Sunlight illumination

To direct light to the v-PV, we employed an aluminum mirror with the size of 20 cm × 20 cm to reflect sunlight from an intensity-tunable solar simulator (Newport©, Solar simulator model 92190) to the PV module. The incline angle and the position of the mirror were adjusted to ensure that the entire PV module was illuminated by the light.

Radiative cooling

In the radiative cooling part, we followed our previous work and designed a liquid-nitrogen based heat sink. In this design, the heat sink is composed of a black aluminum foil immersed in liquid nitrogen, which can be considered as a blackbody at 77 K. Additionally, an aluminum waveguide was installed between the heat sink and the PV module to ensure the maximized thermal radiation coupling efficiency.

V-PV system

In the v-PV system, we employed two mirrors on the two sides of a PV module, both of them inclined at 45°. On the front side of the PV module, an aluminum mirror was employed (see Figure S5 for the measured reflection spectrum). In this case, the incident sunlight can be reflected to the PV module, while the thermal radiation from the front-side of PV module can be directed to the sky. On the backside of the PV module, a spectral selective reflector was employed (see Figure S5A for the measured reflection spectrum). In this case, the thermal radiation from the backside of PV module can be directed to the sky, while it also can prevent the backside of PV module being heated up by the scattered sunlight. We also measured the reflectivity of the PV module using integrating sphere with FTIR, as shown in Figure S5B. One can see that both sides of the PV module show <5% average reflectivity within the wavelength range from 2 to 16 μm, indicating the strong thermal emissivity of the PV module.

Estimation of atmospheric spectral transmissivity under three distinct humidity

The atmospheric spectral transmittance with different atmospheric water columns is estimated by the MODTRAN Demo of Spectral Sciences, Inc.[52] The emissivity/absorptivity of the atmosphere at the zenith angle, θ, can be described by[53]

$$\epsilon_{sky}(\theta, \lambda) = 1 - \left[1 - \epsilon_{sky}(0, \lambda)\right]^{1/\cos\theta} \quad \text{(Equation 9)}$$

where $[1 - \epsilon_{sky}(0, \lambda)]$ is equal to the modeled atmospheric transmission spectrum from MODTRAN. Using this equation, we plot the angle-dependent atmospheric spectral transmittance in Figure 3A and the angle-dependent transmittance at the wavelength of 12 μm in Figure 3B.

COMSOL modeling of corresponding modified PV system designs

To simulate the working conditions of our design in Saudi Arabia, we set the module parameters according to our outdoor experimental design following the model from COMSOL Application Gallery: *Radiative Cooling*[54] and *Sun's Radiation Effect on Two Coolers Placed Under a Parasol*.[55]

By considering the dominant heat transfer phenomenon when a PV module is subjected to ambient environement, we introduced Heat Transfer in Solid (ht) and Surface-to-Surface Radiation (rad) in the Physics section in the COMSOL modeling to simulate the transfer of heat in solids and solar illumination and heat exchange based on radiation. In our simulations, the dimensions of the solar panels and reflectors were determined based on the measured assemblies for outdoor experiments. The position of the sun over time comes from the statistic of ASHRAE 2021 provided by COMSOL and our modeling date is set to Nov. 13th, 2022. Considering the local latitude, the tilt angle of solar panels was set at 22° facing south for the maximized solar irradiance collection efficiency, while the front mirror was defined as an aluminum

mirror with an incline angle of 45° to ensure minimum shadow effect.[56] The rear-side mirror was defined as a spectral selective mirror (unit emissivity in 0~2.5 μm and zero emissivity within infrared range). The front and rear surface of PV modules and the rear surface of reflectors was set as Diffuse Surface. Figure S6 illustrates the temperature profile in Celsius of the modified v-PV system, where the temperature and received solar irradiance was calculated by averaging the value across the entire PV module surface.

Experiments design: Outdoor test

In the outdoor experiment in Figure 4, two sets of PV modules were fixed perpendicular to the ground, while the front and rear-side mirrors were fixed at 45°. The temperature of the PV module was measured automatically using K-type thermocouples attached to the center of the back of the solar panel. The open-circuit voltage and short-circuit current were measured using digital multimeters. The humidity and solar intensity were measured manually using a hygrometer and a power meter simultaneously. Three sets of solar modules were placed in a wind-shield cover by PE film to ensure the minimized convective cooling introduced by the strong local wind.

In the subsequent outdoor experiment shown in Figure 5, to estimate the cooling performance and output enhancement in a real application, we adjusted the installation angles of the solar panels to 22°C and selective reflectors on rear-side to 0°C. The front mirror is still installed at 45°C, which will not block any solar radiation even in winter. In this measurement, the output of the PV module was measured using an PV analyzer (PCE ins., PVA 100 Photovoltaic Moduler Analyzer). To minimize the experimental error introduced by the modules, we tested three identical setup for each designs and calculated the average values. Humidity, wind speed, and solar intensity are measured using a weather station near the ground.

Estimation of the benefits of radiative cooling on PV modules

Based on ref. [57], Time-to-failure (TTF) of PV modules is the length of time that PV modules are expected to last. The threshold of P_{max} loss for TTF we used for calculation here is 20%. TTF data was subjected to the damp heat tests of different temperature and relative humidity conditions, which was estimated using the equation below:

$$\mathrm{TTF} = A * e^{\frac{E_a}{k_B T}} * (RH)^n \quad \text{(Equation 10)}$$

Here A is a pre-exponential factor (6.4×10^{-10} for 20% P_{max} loss); E_a is the activation energy of Si PV module (in this calculation, we refers to ref. [7] and assume E_a to be 0.89 eV; k_B is a Boltzmann constant; T is the operating temperature of the PV module in Kelvin and RH is the relative humidity of environment, both of which are extracted from the experimental results from Figure 5; the value of n is used as −2.2. All parameters except T and RH are chosen based on the SunEdison and literature reports, as summarized in Table S2. The degradation rate is calculated based on the threshold of P_{max} loss (i.e., 20%):

$$\text{Degradation rate} = P_{threshold}/\mathrm{TTF}. \quad \text{(Equation 11)}$$

As shown in Table S2, the TTF of a modified v-PV (22.22 years) is extended by 4.7% compared to a modified h-PV (21.22 years), corresponding to a reduced degradation rate of 0.043%/year. Using a similar estimation process, the TTF of a modified v-PV is also estimated to be extended by 15.7% compared to a modified sv-PV (19.20 years), corresponding to a reduced degradation rate of 0.142%/year.

By further implementing these estimation results into a LCOE comparative calculator developed by NREL,[58] we also calculated the LCOE of different PV designs, as shown in Table S3. The performance and reliability are determined based on our results. Energy yield is calculated based on the P_{max} of each module (P_{max}/working area x 24 x 365). The value of extra component cost of modified v-PV and sv-PV comes from the spectral selective mirror and aluminum mirror in the V-shaped design, which is set to be 15.6 and 7.1 USD/m^2 respectively,[59,60] and the cell cost was set to be 287 USD/m^2.[61] The parameters used for LCOE calculation are listed in Table S3.

As one can see, the LCOE of a modified v-PV module is reduced by 0.0508 USD/kWh compared to a modified h-PV, revealing the benefits introduced by this radiative cooling strategy in modified v-PV modules.